
Article:
Tomlinson, L., Lu, Z.Q., Bentley, R.A. et al. (6 more authors) (2019) Attenuation of doxorubicin-induced cardiotoxicity in a human in vitro cardiac model by the induction of the NRF-2 pathway. Biomedicine and Pharmacotherapy, 112. 108637. ISSN 0753-3322

https://doi.org/10.1016/j.biopha.2019.108637

Biomedicine & Pharmacotherapy 112 (2019) 108637

Contents lists available at ScienceDirect

Biomedicine & Pharmacotherapy

journal homepage: www.elsevier.com/locate/biopha

Attenuation of doxorubicin-induced cardiotoxicity in a human *in vitro* cardiac model by the induction of the NRF-2 pathway

Lauren Tomlinson[a], Zhen Qi Lu[b], Robert A Bentley[a], Helen E. Colley[c], Craig Murdoch[c], Steven D. Webb[d,e], Michael J. Cross[a], Ian M. Copple[a], Parveen Sharma[a,*]

[a] MRC Centre for Drug Safety Science, Department of Clinical and Molecular Pharmacology, University of Liverpool, Liverpool, UK
[b] School of Medicine, University of Queensland, St. Lucia, Queensland, 4006, Australia
[c] School of Clinical Dentistry, University of Sheffield, Sheffield, S10 2TA, UK
[d] Department of Applied Mathematics, Liverpool John Moores University, Liverpool, L3 3AF, UK
[e] EPSRC Liverpool Centre for Mathematics in Healthcare, Department of Mathematical Sciences, University of Liverpool, Liverpool L69 7ZL, UK

ARTICLE INFO

Keywords:
Cardiotoxicity
NRF2
3D models
Anthracycline

ABSTRACT

Dose-dependent cardiotoxicity is the leading adverse reaction seen in cancer patients treated with doxorubicin. Currently, dexrazoxane is the only approved drug that can partially protect against this toxicity in patients, however, its administration is restricted to those patients receiving a high cumulative dose of anthracyclines. Investigations into the mechanisms of cardiotoxicity and efforts to improve cardioprotective strategies have been hindered by the limited availability of a phenotypically relevant *in vitro* adult human cardiac model system. Here, we adapted a readily reproducible, functional 3D human multi-cell type cardiac system to emulate patient responses seen with doxorubicin and dexrazoxane. We show that administration of two NRF2 gene inducers namely the semi-synthetic triterpenoid Bardoxolone methyl, and the isothiocyanate sulfurophane, result in cardioprotection against doxorubicin toxicity comparable to dexrazoxane as evidenced by an increase in cell viability and a decrease in the production of reactive oxygen species. We further show a synergistic attenuation of cardiotoxicity when the NRF2 inducers and dexrazoxane are used in tandem. Taken together, our data indicate that the 3D spheroid is a suitable model to investigate drug induced cardiotoxicity and we reveal an essential role of the NRF2 pathway in cardioprotection providing a novel pharmacological mechanism and intervention route towards the alleviation of doxorubicin-induced toxicity.

1. Introduction

The anthracycline doxorubicin, although first introduced in the 1960s, continues to be a commonly used and highly effective chemotherapeutic drug used to treat both adults and children for a wide range of cancers including Hodgkin's and non-Hodgkin's lymphoma, acute myeloid leukemia, breast and ovarian cancers. However, the dose-dependent cardiotoxic effects of doxorubicin can limit patient exposure and therapeutic efficacy. Even at relative low cumulative doses (200–250 mg/m^2) an increase of 8% of adverse cardiac events has been observed [1], further increasing to 26% with cumulative doses of 550–600 mg/m [2]. In fact, after secondary malignancies the leading cause of mortality in cancer patient survivors is cardiovascular disease (CVD), with an increased eight-fold risk when compared to the general population [3,4]. Side effects of doxorubicin include left ventricular wall stress leading to reduction in the left ventricular ejection fraction (LVEF), ventricular and atrial arrhythmia, chronic cardiomyopathy and congestive heart failure.

Multiple mechanisms have been implicated in both the antineoplastic and cardiotoxic action of doxorubicin, although both remain incompletely understood [1,5]. The antineoplastic mechanisms include the stabilisation and intercalation of doxorubicin with the topoisomerase II-α (TOP2 A)–DNA cleavage complex, which in turn leads to the prevention of DNA break repair, as well as the inhibition of DNA replication in rapidly proliferating cancer cells leading to cancer cell death [6]. Further, doxorubicin has been implicated with the generation of free radicals that cause damage to DNA, cellular proteins and mitochondria. Presently, mechanisms of cardiotoxicity include myocardium injury through the generation of reactive oxygen species (ROS) leading to subsequent membrane damage, impaired mitochondrial function, upregulation of proteins that mediate apoptosis and disruption of calcium (Ca^{2+}) homeostasis causing Ca^{2+} overload that leads to

* Corresponding author.
E-mail address: Parveen.Sharma@liverpool.ac.uk (P. Sharma).

https://doi.org/10.1016/j.biopha.2019.108637
Received 23 August 2018; Received in revised form 28 January 2019; Accepted 28 January 2019

sarcomeric disarray and myofibril deterioration [1,6,7]. This disruption of functioning sarcomeres highlights a potential mechanism for the loss of contractile force that is symptomatic of patients with doxorubicin-associated cardiotoxicity [8–10].

Experimental animal model systems have been and will continue to be instrumental in providing important insights into the molecular basis of cardiotoxicity and CVD. However, it is widely recognised that the physiology of human cardiac cells differs from those of rodents; the most commonly used *in vivo* experimental model [11,12]. Therefore, research into mechanisms of CVD would be strengthened significantly by the availability of *in vitro* models based on human cells. Advances in the ability to generate cardiomyocytes from human embryonic stem cells (hESC-CM) as well as the reprogramming from induced pluripotent stem cells (iPS-CM) [1] have started to alleviate this hurdle and provide researchers with tools to study CVD and test new drugs. However, to date, the stem cells used in CVD research remain in an immature state and are therefore not reflective of the phenotype of adult cardiomyocytes [1]. Indeed, this cellular immaturity was recently exemplified in an *in vitro* study in which dexrazoxane, the only drug approved by the FDA for protection against doxorubicin induced cardiotoxicity, was found to exacerbate the condition in iPS-CM [1,13].

Oxidative stress resulting from an increase in the generation of ROS is one of the most widely cited mechanisms regarding the molecular pathway underlying anthracycline induced cardiotoxicity. However, the administration of generic anti-oxidants has been shown to result in no alleviation of the condition [14,15]. The activation of the transcription factor NF-E2-related factor 2 (NRF2) has been shown to antagonise oxidative stress *via* the upregulation of multiple cytoprotective genes [16,17]. This has stimulated the development of several pharmacological activators of NRF2, including semi-synthetic triterpenoids which have been shown to offer protection against ROS both *in vivo* [18–20] and *in vitro* [21,22], and have subsequently entered clinical trials.

Here, we show *in vivo* like responses in a readily constructible 3D microtissue spheroid in which human cardiomyocytes are grown in combination with human cardiac fibroblasts and endothelial cells. Consistent with this, the spheroids show a concentration-dependent toxicity response to doxorubicin that is reduced in the presence of dexrazoxane. Making use of this mechanistically-relevant model, we show that Bardoxolone methyl (BARD, also known as 2-cyano-3,12-dioxooleana-1,9(11)-dien-28-oic acid methyl ester (CDDO-me)) as well as Sulforaphane, an isothiocyanate from the cruciferous vegetable family, both known NRF2 activators [16,23] can protect against doxorubicin induced cardiotoxicity to a similar extent as dexrazoxane but, have a pronounced synergistic effect when co-administered in the presence of dexrazoxane.

2. Results

2.1. Formation of 3D cardiac spheroids

We formed monoculture 3D cardiac microtissue spheroids comprised of human cardiomyocytes alone and a tri-culture spheroid comprised of human cardiomyocytes, fibroblasts and endothelial cells. Two week-old monoculture cardiomyocyte formed loosely associated spheroids that showed no sign of striation upon immunofluorescent-staining using the cardiomyocyte specific marker α-actinin (Fig. 1A). In contrast, the tri-culture formed tightly associated spheroids as early as day 5 that displayed limited striations in addition to the presence of endothelial cells visualised using CD31 (endothelial cell marker) and extensive fibroblast-generated type I collagen extracellular matrix (Fig. 1B). All markers were retained at 2 weeks in culture (Fig. 1C). Both monoculture and tri-culture spheroids initiated beating after two weeks of culture which coincided with the co-localization of immuno-positive staining for HCN4 and α-actinin, showing localization of pacemaker cells at this time point compared to a more dispersed staining at 5 days (Supplemental Fig. 1). The beating rate of monoculture spheroids was significantly lower (46.8 ± 0.86 bpm) when compared to the tri-culture spheroids (74.8 ± 2.3 bpm; $p = 0.00002$, student's t-test) (Fig. 1D), the latter being more emulative of the beating rate range of a resting human adult heart (60–100 bpm) [24,25].

2.2. Oxygen profiles of spheroids

To ensure that the dimensions of spheroid system permitted an adequate oxygen supply throughout the system we carried out *in silico* predictions of oxygen (O_2) profiles. Spheroids of radii 88 μm (the average radius of spheroids in this study, blue curve/dot in Fig. 2A and B) have only a minimal decrease in O_2 with 21% O_2 at the outer surface decreasing to 16.3% O_2 in the core. The core O_2 % concentration then decreases almost linearly with a further 1% O_2 reduction at the core for each 7.4 μm increase in the spheroid radius. Moreover, hypoxia (O_2 less than 1%) was only predicted in spheroids of radii greater than 190 μm (red curve/dot in Fig. 2A and B and Cii) ensuring that the size of the spheroids used in this study (Fig. 2Ci) have a well-maintained oxygen supply.

2.3. Cellular morphology of 3D microtissues

Since the tri-culture system showed striations and beating rates similar to adult human cardiomyocytes, this model was examined further to confirm cellular morphology. Electron microscopy (EM) images of the two-week spheroids, when the spheroids first initiate beating, showed no evidence of organized cardiac tissue (Supplemental Fig. 2). However, spheroids maintained in culture for five weeks showed extensive α-actinin-positive striations by immunofluorescence (Fig. 3A) and electron microscopy (EM) (Fig. 3B). EM images display evidence of ultrastructure with the alignment of Z-disks and formation of I-, H-, A- and M bands, as well as presence of myofibrils (Mf) (Fig. 3B) and numerous mitochondria (Supplemental Fig. 3). To determine spheroid functionality we examined the activation of cardiomyocyte-expressed ryanodine receptor (RyR2) intracellular calcium (Ca^{2+}) channels in response to caffeine. Quantification of caffeine-induced Ca^{2+} transients showed a significantly ($p = 0.02$, students t-test) increased response in the 5 week spheroids when compared to those seen at the earliest stage of contraction in 2 week-old spheroids (Fig. 3C-E). Blockade of the L-type Ca^{2+} channels with verapamil resulted in termination of Ca^{2+} transients and further stimulation with caffeine following verapamil blockage caused Ca^{2+} release from the sarcoplasmic reticulum by both 2 and 5 week-old spheroids (Fig. 3F, G). In addition, inhibition of Ca^{2+}-ATPase (SERCA) ion-transport activity by the addition of thapsigargin led to the cessation of caffeine-induced Ca^{2+} transients due to depletion of Ca^{2+} from the sarcoplasmic reticulum (Fig. 3H, I). Taken together these results indicate the presence of a functional sarcoplasmic reticulum in our 3D spheroid system.

2.4. Mass spectrometry analysis of cardiac cell development

We next, applied global mass spectrometry, database searching and statistical filtering at the peptide and protein level (< 1% FDR), followed by relative quantification based on spectral counts on both 5 day and 5 week tri-culture spheroids to confirm the presence of known proteins and to identify previously unannotated proteins differentially regulated upon cellular development. Analysis of three biological repeats resulted in 2497 human protein identifications with a final set of 1766 passing selection criteria (< 1% FDR and ≥ 2 peptides per protein identified) (Supplemental Table 2). Comparative proteomics using Progenesis identified 1126 differentially expressed protein clusters ($p \leq 0.05$, ANOVA and/or 1.5 ≥ fold change; Fig. 4A). The hallmarks of cardiac development is an increase in structural proteins involved in the adult myocardium, as well as proteins involved in calcium handling and cardiac contraction. We observed a significant increase ($p < 0.05$) in expression of the structural proteins; sarcomeric α-actinin, β-myosin, myosin binding protein C (MYBPC3), as well as an increase in myosin light chain that is predominantly seen in adult ventricular tissue (MLC-

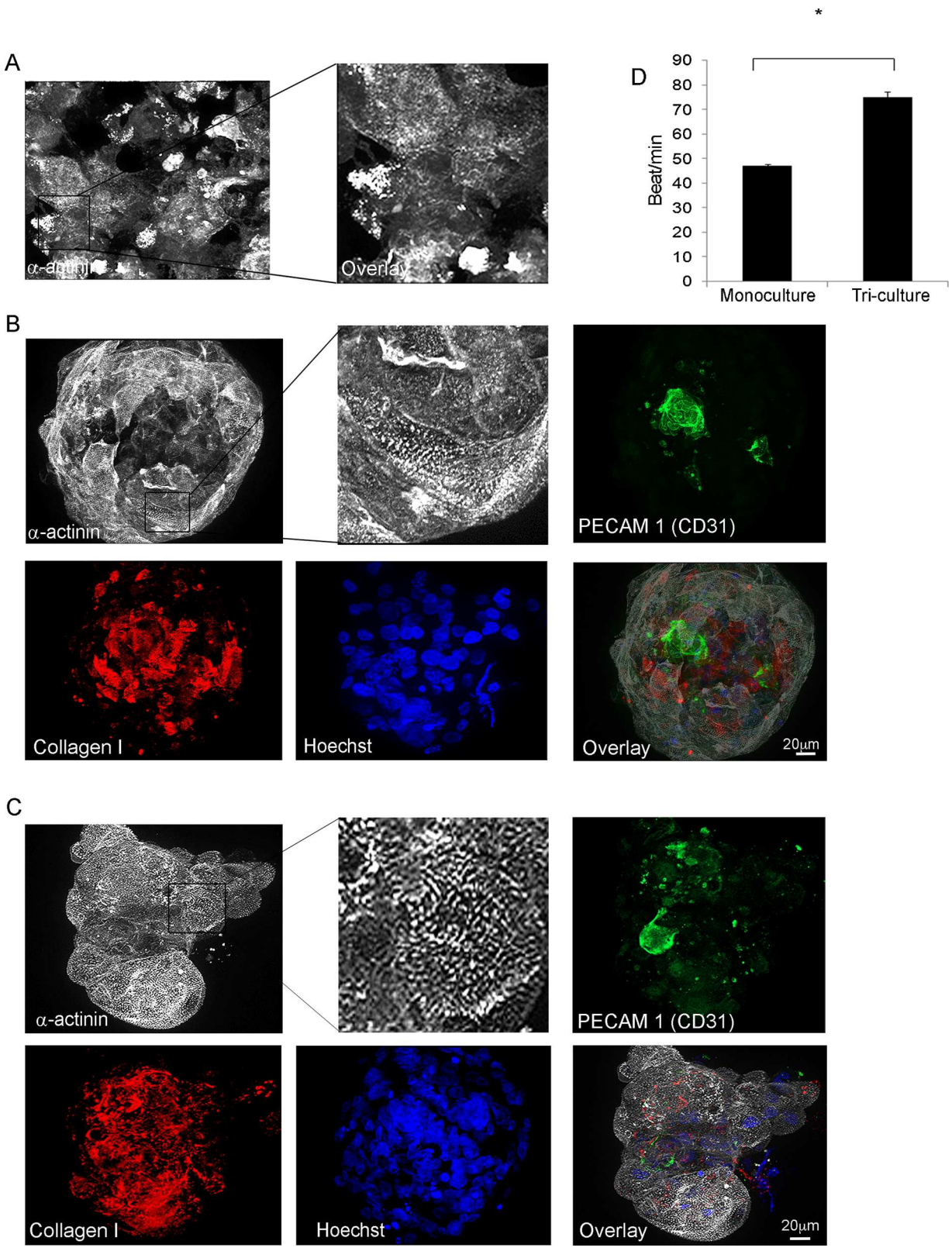

Fig. 1. Verification of 3D cardiac spheroids structure A) Immunofluorescence of 2 week mono-culture spheroids show no striations after staining with α-actinin B) immunofluorescence of tri-culture spheroids at 5 day and C) 2 weeks show visible striations which are retained as seen with α-actinin antibody, fibroblast matrix stained with collagen I and endothelial cells with CD31 staining. All immunofluorescence images were counterstained with Hoechst (nuclei), D) Beating rate of spheroids shows significant difference between tri-culture and monoculture spheroids (data shown as mean of beating rate ± SE, n = 10 (3 independent runs); $p < 0.05$, student's t-test).

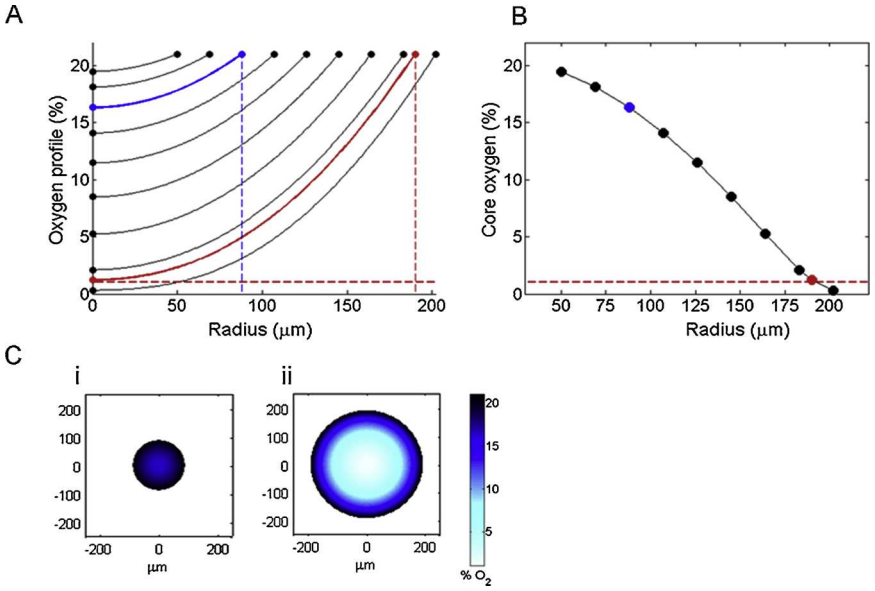

Fig. 2. Oxygen profile of spheroids A) Graphs show the oxygen profile of spheroids with differing radii with the outer core exposure set at atmospheric 21%. Blue curve represents average radii of spheroids used in this study and red indicates size that would lead to a hypoxic core B) Graph of percentage oxygen distribution at the core of the spheroids blue dot is the percentage in the spheroids used in this study and red in a hypoxic core C) Heat profile of oxygen distribution of size of spheroids i) used in this study ii) predicted to have a hypoxic core (For interpretation of the references to colour in this figure legend, the reader is referred to the web version of this article).

2v, MLC1SB) [26,27] and adult atrial tissue (MLC-2a) [27,28] in 5 week compared to 5 day spheroids (Fig. 4B). This trend was also seen in calcium handling proteins involved in cardiac contractions; namely Ca^{2+}ATPase (SERCA), phospholamban (PLN), Ryanodine receptor (RyR2) and the sodium potassium ATPase (Na/K ATPase) (Fig. 4B). In addition, we observed a significant ($p = 0.0027$, ANOVA) increase in expression of Tmem65, a recently identified maturation marker of cardiomyocytes [29]. Gene ontology (GO) analysis calculated using DAVID (http://david.abcc.ncifcrf.gov) of the significantly up regulated proteins in the 5 week spheroids showed enrichment in processes associated with cardiac development such as *ion transport* ($n = 35$, $p \leq 0.05$), *muscle contraction* ($n = 29$, $p \leq 0.05$) and *heart development* ($n = 18$, $p \leq 0.05$; Fig. 4C). Interestingly, in agreement with the terminally differentiated nature of mature cardiac cells, the GO term analysis of the significantly down-regulated proteins included a decrease in *cell motion* ($n = 31$, $p \leq 0.05$), *cell cycle process* ($n = 24$, $p \leq 0.05$) and *cell morphogenesis* ($n = 17$, $p \leq 0.05$; Fig. 4C).

Ingenuity pathway analysis (IPA) identified *cardiovascular system development and function* as the top biological functional pathways ($n = 72$, $p \leq 0.005$) with the key nodes and their corresponding proteins shown in Fig. 4D. IPA analysis highlighted pathways involved in the development of cardiac tissue between pre- and post-beating cardiac spheroids. It further highlighted a complex of proteins that were upregulated in cardiac contraction, which included those identified in Fig. 4D, but extended this data to include other known regulators such as histidine-rich calcium binding protein (HRC), a recently identified SERCA binding protein [30,31], as well as PRKACA and CAMK2D. Upstream analysis identified known cardiac transcription factors; MYOCD, GATA4, HAND2, and TBX5 to be activated, inducing the up and down-regulation of proteins involved in cardiac development and contraction [32] (Fig. 4E).

To gain a better understanding of proteins that were significantly increased in cardiac development we compared all 416 proteins (≥ 1.5 fold and $p \leq 0.05$ in the 5 week spheroid) to publically available human adult heart microarray data [33] and found that 251 proteins were identified with 3-fold intensity above global median. A comparison to our previously determined chamber specific proteins identified 11 atria specific markers and 30 ventricle specific markers enriched within this dataset [34]. Finally, in order to determine which proteins have previously been implicated in disease, we searched our developmentally regulated proteins against previous links to cardiac function on the basis of phenotype ontology (http://www.informatics.jax.org). This identified 75 previously implicated proteins thereby identifying 341 previously phenotypically uncharacterized human cardiac associated proteins (Fig. 4F).

2.5. Doxorubicin induced cardiotoxicity

Since 5 week old spheroids showed greater *in vivo* like morphology, we used them to investigate doxorubicin induced cardiotoxicity. Lightsheet-based immunofluorescence microscopy (Zeiss LightSheet Z.1) showed that doxorubicin penetrated cells throughout the spheroid microtissue and was not restricted to the exposed surface area resulting in a homogeneous reporter system (Fig. 5A). Spheroids displayed a concentration-dependent loss of cell viability in response to doxorubicin, resulting in an IC_{50} of 0.35 μM (Fig. 5B). Moreover, pre-treatment of cells with the cardioprotectant dexrazoxane diminished the toxic effect of doxorubicin leading to an increased IC_{50} of 6.6 μM (Fig. 5B). We next sought to assess the protective effects of activating NRF2, by pre-treating cells with bardoxolone methyl (from here on known as CDDO-me) prior to treatment with 0.001 mM doxorubicin. Under these conditions there was a significant 2-fold ($p \leq 0.05$) increase in cell viability (Fig. 5C). Interestingly, when cells were pre-treated with both dexrazoxane and CDDO-me a significant 5-fold synergetic cardioprotective response ($p \leq 0.005$) was seen when compared to the doxorubicin treated cells and also a significant ($p \leq 0.05$) increase in viability compared to dexrazoxane administered alone (Fig. 5C). In order to confirm a reduction in the oxidative stress inferred by doxorubicin we measured levels of reactive oxygen species (ROS) which revealed a significant decrease ($p \leq 0.05$) in ROS levels in the presence of dexrazoxane and CDDO-me independently (Fig. 5D) but to a greater extent ($p \leq 0.01$) when administered in tandem (Fig. 5D). To further confirm the protective effect of NRF2 induction we pre-incubated spheroids with an alternative pharmacological activator, sulforaphane, prior to doxorubicin treatment. This consistently showed a significant ($p \leq 0.05$) increase in cell viability and a significant synergetic cardioprotective response ($p \leq 0.005$) when incubated together with dexrazoxane (Fig. 5E). No significant change of basal levels of ATP (Supplemental Fig. 4A) or ROS (Supplemental Fig. 4B) were seen in the presence of NRF2 stimulants in the absence of a cellular challenge by doxorubicin indicating that the NRF2 inducers modulated ATP only in the presence of cellular distress by doxorubicin. In keeping with previously observed results [1] spheroids in the presence of doxorubicin showed a loss of integrity and increased disarray within the sarcomeric structure of the cardiomyocytes (Fig. 5F). However, in the presence of dexrazoxane and CDDO-me, morphological analysis showed the retention of sarcomeric structures (Fig. 5F), consistent with the observed cardioprotective effects of the drug combination.

In order to directly ascertain that the pre-treatment with both the

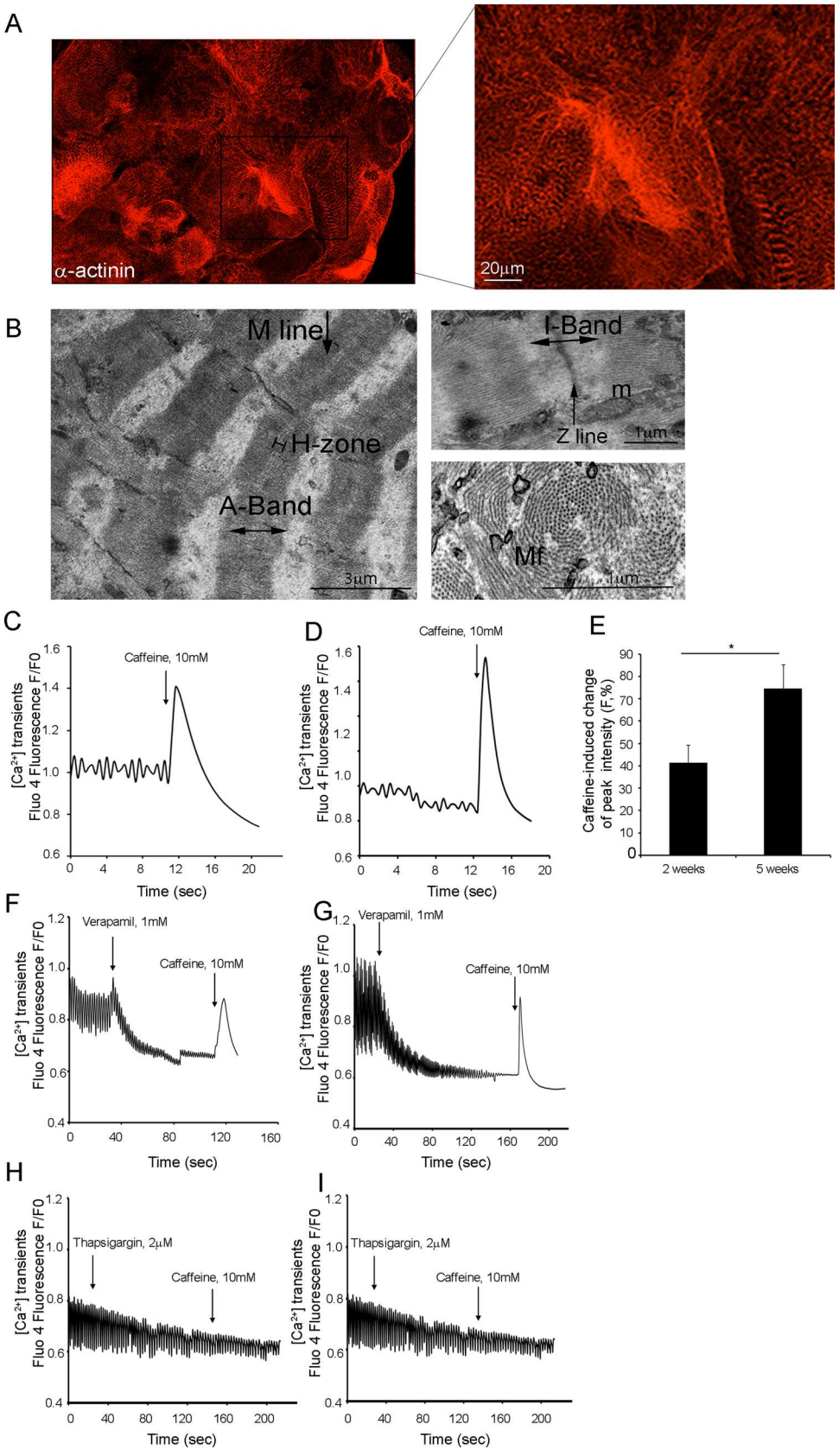

Fig. 3. Morphological and functional assessment of spheroids A) Immunofluorescence staining at 5 weeks show extensive striations (α-actinin, red), B) Electron microscopy images of spheroid ultrastructure showed sarcomeres; Z disks, black arrow; H zones, M lines and I-bands; mitochondria (m) and the presence of myofibril bundles (Mf). Representative traces of Ca^{2+} release in response to 10 mM caffeine in C) 2 week spheroids and D) 5 week spheroid. E) Percentage caffeine-induced change of peak fluorescence intensity at 2 and 5 weeks (graph indicates mean ± s.e after normalizing the peak fluorescence intensity before caffeine administration) * denotes significant difference ($p = 0.02$, $n = 3$, students t-test). Representative traces of Ca^{2+} release in response to 1 mM verapamil before and after administration of caffeine at F) 2 weeks and G) 5 weeks. Representative traces of Ca^{2+} release in response to 2 μM Thapsigargin before and after administration of 10 mM caffeine at H) 2 weeks and I) 5 weeks ($n = 3$). F, fluorescence intensity; F0, fluorescence intensity at baseline; F/F0, F normalized by F0. (For interpretation of the references to colour in this figure legend, the reader is referred to the web version of this article).

drugs did not affect the antineoplastic efficacy of doxorubicin, we administered the corresponding concentrations to AU565 breast cancer cells and showed no significant difference in cell viability when compared to the administration of doxorubicin alone (Fig. 5G).

2.6. Role of NRF2 in cardioprotection

To confirm that CDDO-me effectively activated NRF2 signalling in cardiac spheroids we determined the expression levels of NRF2 target

genes by quantitative PCR (qPCR). This analysis showed a significant synergistic induction of established NRF2 targets NQO1, SRXN1, AKR1C1 and TXNRD1 in the presence of dexrazoxane and CDDO-me (Fig. 6A). To confirm the involvement of the NRF2 pathway in the cardioprotective mechanism we next used ML385, a small molecule inhibitor of NRF2 [35]. Western blot analysis showed a significant dose dependent decrease in NRF2 levels at the protein level (Fig. 6B and Supplemental Fig. 5) as well as a decrease of downstream target

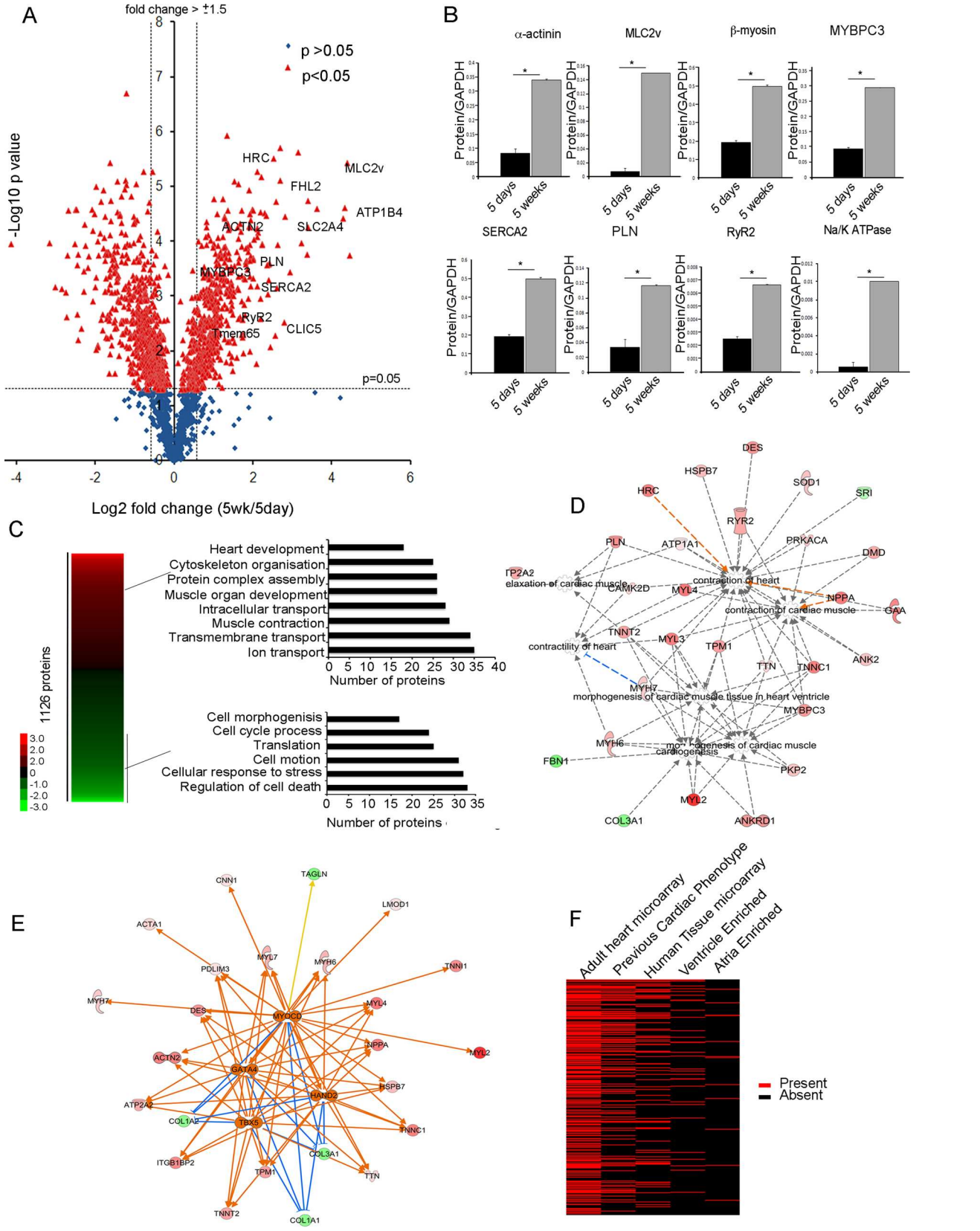

(caption on next page)

Fig. 4. Mass spectrometry analysis of spheroid development A) Volcano plot of the total proteins identified at 5 day and 5 weeks plotted with *p-value* against the log fold change from 3 independent experiments. Differentially expressed proteins (*p-value* ≤ 0.05) are shown in red. Horizontal line represents *p-value* = 0.05 and vertical lines represent fold change of ± 1.5 fold, B) Changes in levels of key proteins involved in cardiac development relative to GAPDH C) Gene Ontology (GO) term analysis of differentially expressed proteins (*p-value* ≤ 0.05), red represents upregulated and green down regulated proteins, D) IPA analysis of *cardiovascular system development and function* further indicated enrichment of proteins involved in development and contraction of the heart, red represents upregulated and green down regulated proteins, E) IPA analysis of upstream regulators identified key transcription factors involved in cardiac development, orange represents significantly up regulated proteins and pathways, blue represents down regulated pathways and green represents down regulated proteins. F) Heatmap of 416 significantly up regulated proteins (≥ 1.5 fold and p ≤ 0.05 in the 5 week spheroid) by 3-fold intensity above global median in the adult and tissue microarray, had a previously known cardiac phenotype and were enriched in our previous atria [34] and ventricle proteome [29,34], red represents presence and black absence of proteins. (For interpretation of the references to colour in this figure legend, the reader is referred to the web version of this article).

TXNRD1 (Fig. 6B). Treatment of cells in the absence of doxorubicin showed no significant change in viability of cells upon treated with ML385 alone (Fig. 6C) or in the presence of CDDO-me or Sulforaphane (Supplemental Fig. 6). In the presence of doxorubicin, ML385 incubation of cells pre-treated with either CDDO-me or sulforaphane led to no significant protection against doxorubicin induced cardiotoxicity (Fig. 6D).

3. Discussion

Chemotherapy-induced cardiotoxicity is a serious concern for established as well as newer anticancer agents [36]. The relevance of *in vitro* human cardiac models for research into cardiac disease and toxicity clearly depends on an ability to emulate the phenotype of in *vivo* cardiac tissue as closely as possible. Efforts to promote greater physiological relevance in multiple cells types have suggested that 3D systems have improved functionality and cellular morphology when compared to their 2D counterparts [37–40]. With this in mind, we used a multi-cell type 3D cardiac spheroid model to investigate doxorubicin induced decrease in viability and structural integrity. In keeping with patient observations dexrazoxane treatment showed cardioprotection in this 3D microtissue system leading to an increase in cell viability and the maintenance of structural integrity in the presence of doxorubicin. This clinically-relevant observation, has not previously been reported for monolayer iPSC derived cardiomyocytes with suggestions that this resulted from cellular immaturity [1]. We show NRF2 stimulated cardioprotection to similar levels as dexrazoxane and further showed synergistical cardioprotection against doxorubicin induced toxicity with the co-administration of dexrazoxane and two NRF2 inducers namely CDDO-me and sulforaphane. Used together these drugs showed a greater significant increase in cell viability, greater decrease in the amount of ROS generated and restoration of sarcomeric structural integrity when compared to that seen with dexrazoxane alone. This coincided with a significant increase in downstream targets of NRF2, which is regarded as a master regulator of defence against the effects of oxidative stress [41]. The cessation of a significant cardioprotective effect in the presence of the small molecule NRF2 inhibitor ML385, further emphasized the involvement of NRF2 in doxorubicin-induced cardiotoxicity.

The multi-cell type 3D cardiac system described here is an easily reproducible model of cardiac cell development. In many of the current systems, cardiomyocytes are used in isolation and therefore not subjected to the physiological cross talk and signaling between the different cell types within the human heart. Indeed, it has previously been noted that greater *in vitro* cardiomyocyte development occurs in the presence of non-cardiomyocyte cells [42,43]. Although the 3D system initiated cellular beating activity and showed the development of striations by 2 weeks, EM analysis showed that ultrastructure development occurred after 5 weeks. The responsive behavior of Ca^{2+} handling proteins through stimulation and inhibition by caffeine, thapsiargin and verapamil confirmed that this system is functionally active. Taken together these data indicate the presence of a functional sarcoplasmic reticulum within the multi-cell type spheroid microtissue system. However, it must be noted that although this system exhibits key features of cardiac tissue, it remains somewhat electrically immature as is evident from its spontaneous beating, since fully mature cardiac cells are quiescent [44] and therefore future research will be guided into a more in-depth understanding of this parameter. The small size (~88 μm in diameter) of the spheroid ensures sufficient oxygen delivery as previously noted for the engineered biowire structure, which have a radius of approximately 300 μm [45] and therefore these cardiac spheroids can be maintained in culture without perfusion.

We determined that the majority of proteins found in the MS analysis of the multi-cell type spheroid microtissue system were previously found in publically available adult heart microarray data [33]. This included an increase in adult isoforms of an extensive range of sarcomeric proteins including β-myosin, Troponin T- I and C- proteins, tropomyosin, actin, myomesin, obscurin, nebulette, MLC2v that are essential for mechanical force generation [26,44]. In addition, we observed sarcomeric proteins previously not seen in 3D cultures such as alpha-sarcomeric protein and myosin-binding protein C [44]. We also found an increase in key proteins involved in contraction including RyR2, SERCA2 and PLN, as well as a significant increase in expression of Tmem65, an essential protein in cardiac contraction [29].

To the best of our knowledge this is the first study in which dexrazoxane has been administered in tandem with the NRF2 activators CDDO-me and sulforaphane to monitor their cardioprotective potential. Dexrazoxane, the only FDA approved cardioprotectant has been shown in clinical trials to be effective in multiple cancer modalities in limiting the cardiotoxic effect seen by anti-cancer drugs [46–49]. However, despite this, it is currently only administered to women with metastatic breast cancer who have received a cumulative dose of anthracycline of 300 mg/m^2 or higher [3]. Initially, evidence from short-term clinical trials suggested that administration of dexrazoxane may increase the risk of secondary malignancies or decrease the antineoplastic efficacy of the anti-cancer drugs. These claims however were challenged in long-term follow ups [3] with some studies now supportive of the concomitant administration of dexrazoxane and anthracyclines to prevent cardiovascular complications [49,50]. However, despite this the European Medicines Agency declined widening the indication of dexrazoxane to all cancer patients and dexrazoxane remains only available to those patients who are expected to receive high cumulative doses of anthracyclines [50] even though low dose exposure has been associated with cardiac damage [1,51,52]. With this in mind, our study shows that for those patients on low dose anthracyclines to whom dexrazoxane remains unavailable, an alternative means of cardioprotection may be through the stimulation of the NRF2 pathway. We show here that CDDO-me (Fig. 6A) or sulforaphane (Fig. 6C) used alone increased cell viability and decreased ROS production (Fig. 6B) to the same efficiency as dexrazoxane alone.

Several mechanisms of dexrazoxane cardioprotection have been proposed including its ability to be a strong metal-chelating agent which chelates free iron thereby preventing the formation of the iron-anthracycline complexes that are responsible for the generation of superoxide free radicals *via* redox reactions [53]. CDDO-me and sulforaphane on the other hand are potent inducers of the NRF2 pathway, a major cellular defence mechanism against oxidative stress. Used at low concentrations (1–100 nM) CDDO-me is cytoprotective but can induce apoptosis when administered at high concentration [54]. Here, we show that a low concentration of CDDO-me is cardioprotective but does not alter the chemotherapeutic efficacy of doxorubicin towards breast cancers cells (Fig. 5G).

This study clearly shows that dexrazoxane treatment does not influence NRF2 activation (Fig. 6A) but does significantly decrease ROS production (Fig. 5D) and that CDDO-me when added alone also significantly decreases the ROS production to an equivalent degree (Fig. 5D) potentially through activation of downstream antioxidant genes including SRXN1, TXNRD1 [55] and NQO1 (Fig. 6A) [56]. The addition of CDDO-me + dexrazoxane in tandem further show a greater significant improvement in viability and decrease in ROS than either reagent alone. However, the addition of CDDO-me + dexrazoxane does not significantly decrease the levels of ROS beyond that of dexrazoxane or CDDO-me alone suggesting that addition of CDDO-me in tandem with dexrazoxane may promote additional protection *via* the NRF2

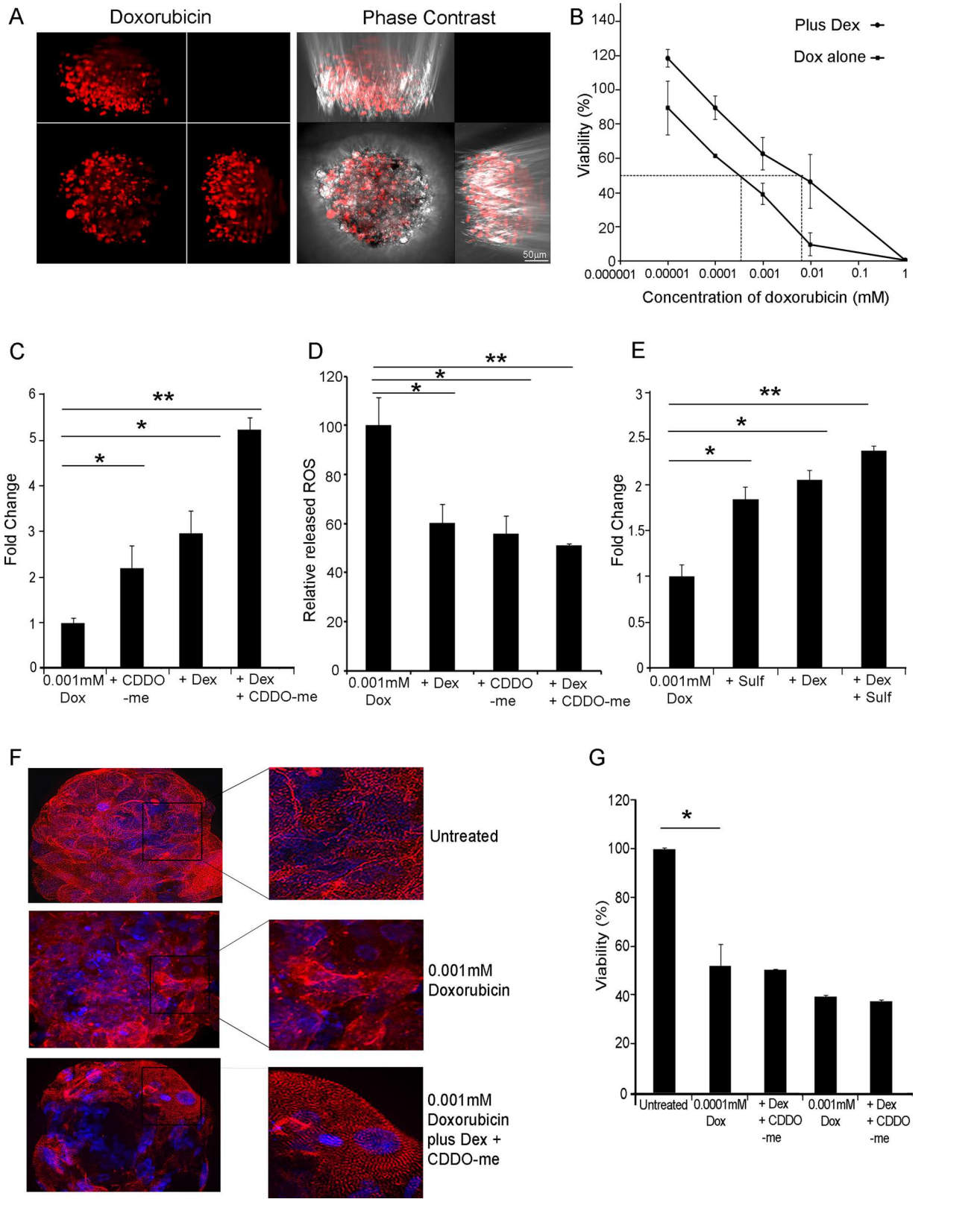

(caption on next page)

Fig. 5. Synergistic cardioprotection against doxorubicin toxicity by dexrazoxane and CDDO-Me A) Immunofluorescence and phase contrast Lightsheet microscopy images of doxorubicin (red) using 0.001 mM doxorubicin after a 30 min incubation. Three planes (x, y and z) of images show penetration of drug throughout spheroid B) Assessment of cell viability at increasing doses of doxorubicin in 3D human spheroids in the presence and absence of 100 μM Dexrazoxane (Dex). Data normalised to vehicle only control and vehicle + 100 μM Dex respectively, graph represent mean ± SE, n = 3 C) Fold change of cell viability seen in the presence of 0.001 mM doxorubicin. Significant changes in viability seen upon pre-treatment with 100 μM Dex and 100 nM CDDO-me administered independently and in tandem. * $p \leq 0.05$; ** $p \leq 0.005$ students t-test, n = 3. D) Fold change in ROS revealed a significant decrease (*$p \leq 0.05$) in ROS levels in the presence of dexrazoxane and CDDO-me independently but to a greater extent (**$p \leq 0.01$) when administered in tandem. E) Significant changes in viability seen upon pre-treatment with 100 μM Dex and 10 μM sulforaphane administered independently and in tandem. * $p \leq 0.05$; ** $p \leq 0.005$ students t-test, n = 3. F) Structural integrity was monitored using α-actinin (red) showed a dose-dependent decrease in structure that was partially rescued in the presence of Dex and CDDO-me. G) Viability of AUG565 breast cancer cells showed a significant decrease in viability in the presence of 0.001 mM and 0.0001 mM Dox. Pre-treatment with 100 μM Dex and 100 nM CDDO-me in tandem showed no significant change to those treated with Dox alone (graphs represent mean ± SE, n = 3 for all experiments) (For interpretation of the references to colour in this figure legend, the reader is referred to the web version of this article).

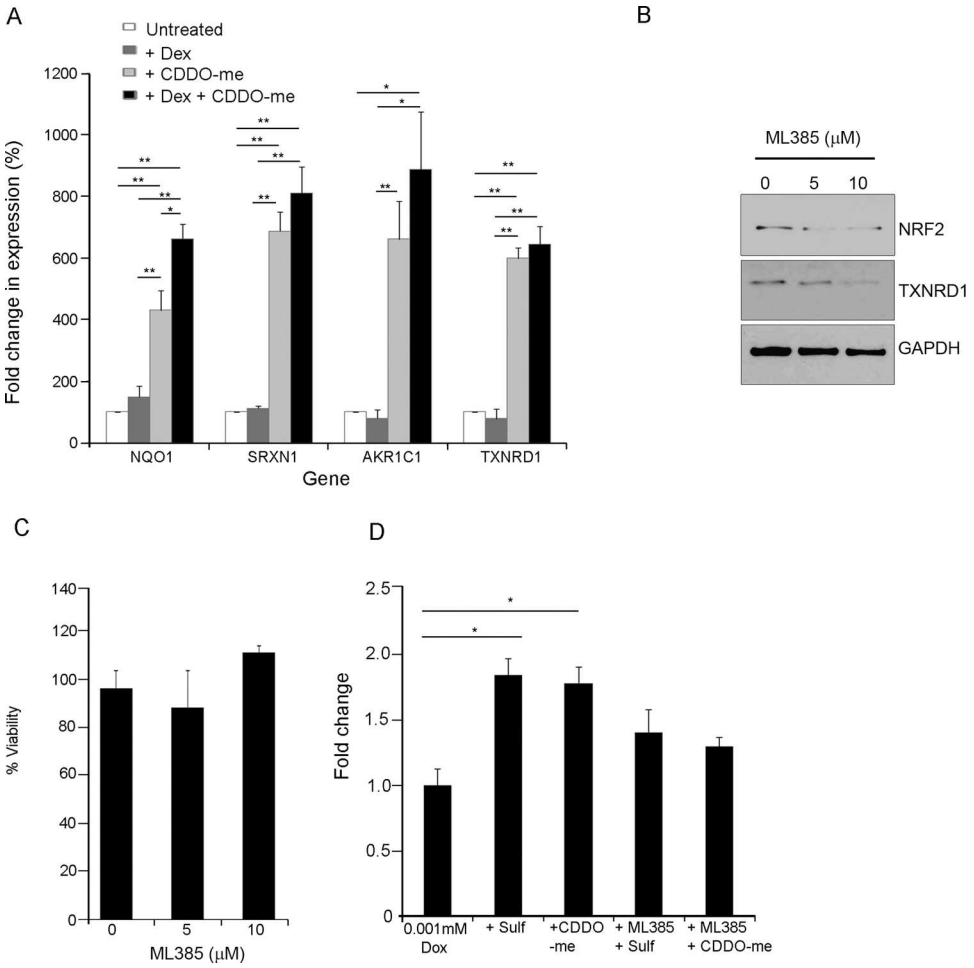

Fig. 6. Role of NRF2 in the cardioprotective effects of dexrazoxane and CDDO-Me A) qPCR analysis of established *NRF2* targets *NQO1*, *SRXN1*, *AKR1C1* and *TXNRD1* in cells treated with 100 μM dexrazoxane and/or 100 nM CDDO-me (* $p \leq 0.05$; ** $p \leq 0.01$, Anova, n = 3 graph represent mean fold change ± SE) B) Immunoblot analysis of protein levels of NRF2 and downstream target TXNRD1 in the presence of ML385 inhibitor. C) Viability of spheroids in the presence of ML385 alone showed no significant difference at increased inhibitor doses (graph represent mean ± SE n = 3). D) Fold change of cell viability seen in the presence of 0.001 mM doxorubicin. Significant changes in viability were seen upon pre-treatment with 10μM sulforaphane and 100 nM CDDO-me in the absence of inhibitor (* $p \leq 0.05$ graph represent mean ± SE, n = 3). However, no significant change was seen in the presence of ML385 inhibitor.

pathway through a secondary mechanism of perhaps by increasing the glutathione levels as previously suggested [57].

Several clinical trials have focused on the preventive and therapeutic activities of CDDO-me against a range of cancers [21] with initial analysis showing growth suppression of malignant cells at higher doses of CDDO-me with no reported severe adverse reaction [21,54]. Amongst several completed and ongoing clinical trials of CDDO-me, only the BEACON trial in stage 4 chronic kidney disease patients has been terminated due to an increase in the frequency of cardiac events (to 8.8%) when compared to placebo [58]. However, post-hoc analysis on this patient population determined those who suffered cardiac events had previously been hospitalised for heart failure and exhibited elevated brain natriuretic peptide (BNP) levels. Those with no previous history of heart failure showed rates of adverse cardiac events similar to those seen in the placebo group (2.0%) [59]. Therefore, it is unlikely that the combined use of dexrazoxane and CDDO-me would cause cardiac events in a suitably stratified patient population. Sulforaphane, has previously been implicated as cardioprotective in cultured rat cardiomyocytes [60] and phase II clinical trials in men with prostate cancer have deemed it a safe treatment although with limited efficacy in this population [61].

To mitigate the complex cardiotoxic action of doxorubicin, a multi-mechanistic cardioprotective approach is required. Since the administration of dexrazoxane to patients receiving a low dose of anthracyclines is restricted, alternative cardioprotective methods must be developed as cardiovascular damage in these patients is well documented. In this study we have demonstrated the potential of exploiting cardioprotective effects of NRF2 induction to minimise doxorubicin induced oxidative stress. We further demonstrate a synergistic protective effect when both dexrazoxane and CDDO-me are administered in tandem. Dexrazoxane, CDDO-me and Sulforaphane have been independently assessed in clinical trials, but this study highlights the need for further investigations into the value of co-administration as a novel strategy to overcome anthracycline induced cardiotoxicity.

4. Methods

4.1. Spheroid formation

Tri-culture spheroids were formed in ultra-low adhesion plates (ULA; Corning) by mixing human embryonic stem cell-derived cardiomyocytes (GE healthcare), human cardiac fibroblasts (Promocell) and human cardiac endothelial (Promocell) cells at a ratio of 4:2:1. A maximum of nine passages were permitted for the fibroblasts and endothelial cells, whereas the cardiomyocytes were used directly from the purchased vial. A total of 500 cells were pipetted into each well of a 96-well plate and cells were cultured in a 1:1 v/v ratio of RPMI (Sigma) media supplemented with B27 (Gibco) and endothelial cell media (MV2, Promocell). Spheroids generated from stem cell-derived cardiomyocytes alone were formed using a total of 1000 cells per well in 96-well ULA plates with RPMI media supplemented with B27 [62]. Spheroids were then allowed to mature until age required for experimentation.

4.2. Immunofluorescence

Spheroids were fixed in 4% paraformaldehyde for 1 h at 4 °C, incubated in permeabilisation buffer (0.5% Triton-X-100, 0.1% Tween-20 in TBS) overnight and blocked in blocking buffer (3% BSA, 0.1% Triton-X-100, 0.1% Tween-20 in TBS) for 2 h at room temperature. Primary antibodies were diluted in blocking buffer and incubated with the spheroids overnight at 4 °C. Spheroids were then washed three times with permeabilisation buffer at room temperature before incubation with secondary antibodies diluted in blocking buffer overnight in the dark at 4 °C. Hoechst and Phalloidin (Thermo Fisher) counterstains were diluted in permeabilisation buffer and incubated with the spheroids for 1 h at room temperature. Spheroids were mounted onto a glass slide with ProLong gold (Thermo Fisher) anti-fade reagent, sealed with a coverslip and images taken using a Zeiss Axio Observer microscope with Apo Tome. Primary antibodies used included: α-actinin (1:400, Thermo Fisher, MA122863, Lot#PA1809212 H), CD31 (1:100, R&D systems, AF806, Lot# DGX0314111), Collagen I (1:100, Abcam, ab21286, Lot# GR211492-4), HCN4 (1:50, Alomore Labs, APC-052, Lot# APC052 AN1725) and Vimentin (1:100, Abcam, ab11256). Drug penetration was recorded using a Zeiss Lightsheet Z.1 microscope as previously described [38].

4.3. Mass spectrometry

Approximately 100 spheroids at either 5 days or 5 weeks were suspended in 160 µl of 25 mM ammonium bicarbonate; 10 µl of 0.05% Rapigest (Waters, Manchester) was added and spheroids shaken at 550 rpm for 10 min at 80 °C. The samples were reduced by the addition of 10 µl of 60 mM Dithiothreitol (DTT) with incubation at 60 °C for 10 min and then alkylated by the addition of 10 µl of 180 mM iodoacetamide at room temperature for 30 min in the dark. Trypsin (Promega UK Ltd., Southampton, proteomics grade) 2 µg was added to the samples followed by overnight incubation on a rotating mixer at 37 °C. The digestion was terminated and Rapigest removed by acidification using 1 µl of trifluoroacetic acid (TFA) with incubation at 37 °C for 45 min followed by centrifugation at 15,000 x g for 15 min. For LC–MS/MS analysis, a 10 µl injection was analysed using an Ultimate 3000 RSLC nano system (Thermo Scientific, Hemel Hempstead) coupled to a QExactiveHF mass spectrometer (Thermo Scientific). The sample was loaded onto the trapping column (Thermo Scientific, PepMap100, C18, 300 µm × 5 mm), using partial loop injection, for seven minutes at a flow rate of 4 µl/min with 0.1% (v/v) formic acid (FA). The sample was resolved on the analytical column (Easy-Spray C18 75 µm × 500 mm 2 µm column) using a gradient of 97% A (0.1% formic acid) 3% B (99.9% ACN, 0.1% formic acid) to 70% A 30% B over 120 min at a flow rate of 300 nl/min. The data-dependent program used for data acquisition consisted of a full-scan 60,000 resolution MS scan (AGC set to 3e6 ions with a maximum fill time of 100 ms) the 18 most abundant peaks were selected for MS/MS using a 30,000 resolution scan (AGC set to 1e5 ions with a maximum fill time of 45 ms) with an ion selection window of 1.2 *m/z* and a normalised collision energy of 28. To avoid repeated selection of peptides for MS/MS the program used a 30 s dynamic exclusion window.

4.4. Proteomic analysis

The MS data was processed using Progenesis Q.I. for Proteomics, version 2 (Nonlinear Dynamics, Newcastle upon Tyne, UK). Samples were aligned according to retention time using a combination of manual and automatic alignment. Default peak picking parameters were applied and features with charges from 1^+ to 4^+ containing three or more isotope peaks were retained. Database searching was performed using Mascot (Matrix Science, London, UK) against UniHuman Reviewed and UniMouse databases. A Mascot Generic File, created by Progenesis, was searched against UniHuman Reviewed database. A fixed carbamidomethyl modification for cysteine and variable oxidation modification for methionine were specified. A precursor mass tolerance of 10 ppm and a fragment ion mass tolerance of 0.01 Da were applied. The results were then filtered to obtain a peptide false discovery rate of 1%.

4.5. Ca^{2+} imaging

Ca^{2+} transients were measured utilizing the Ca^{2+} indicator Fluo-4 (Thermo Fisher). Briefly, spheroids were incubated with 5 µM Fluo-4 AM for 30 min at 37 °C after which they were washed twice with dye-free medium and placed back into the incubator for 30 min. A Zeiss Axio Observer microscope was used to measure the fluorescence intensity of Fluo-4 AM treated with or without different pharmacological agents.

4.6. Cell viability

3D microtissue spheroids were incubated with varying concentrations of doxorubicin (Selleck Chemicals) for 48 h and cell viability measured using a CellTiter-Glo Luminescent Cell Viability Assay (Promega) as described by the manufacturer's instructions. 100 µM Dexrazoxane was added 3 h and 100 nM CDDO-me, 10 µM sulforaphane and 10 µM ML385, 24 h prior to doxorubicin incubation.

4.7. In silico estimates of spheroid O_2

A reaction-diffusion equation was used to estimate the oxygen profiles within the spheroids (full details in supplementary material). A Michaelis-Menten oxygen uptake term was assumed with maximal oxygen consumption rates (Vmax) for the three cell types taken from a study by Sekine et al. [63] which estimated oxygen consumption rates of 1.97×10^{-16}, 5.28×10^{-17}, 6.11×10^{-17} mol/s/cell, respectively, for human iPSC-CM, cardiac fibroblasts (FB) and human cardiac microvascular endothelial cells (EC). The Michaelis-Menten half maximal parameter (Km) and the rate of oxygen diffusion within the spheroid were taken to be 6.24×10^{-3} mol/m^3 [64] and 6.33×10^{-10} m^2/sec [65], respectively. Cell densities were calculated using the average spheroid radius of 88 µm which comprises of a total of 498 cells in a mixed ratio of 4:2:1 for CM:FB:EC (285:142:71 cells) – giving 9.89×10^{13}, 4.97×10^{13}, 2.487×10^{13} cells/m^3 for CM, FB and EC cells, respectively. These same cell densities were then assumed for all spheroid radii considered. The oxygen concentration at the spheroid boundary was fixed at 21% for each spheroid radii. Radial spherical symmetry was assumed and the steady state oxygen profiles for the spheroid interiors were calculated for spheroid radii ranging from 50 to 200 µm.

4.8. Quantitative PCR

Total RNA was isolated from vehicle and drug treated spheroids using the RNeasy mini kit (Qiagen), as per the manufacturer's instructions. cDNA was synthesized using a GoScript cDNA synthesis kit

(Promega), as per the instructions provided for a 96 well plate format. Quantitative PCR (qPCR) analysis of *NRF2*, NAD(P)H dehydrogenase quinone 1 (*NQO1*), Sulfiredoxin-1 (*SRXN1*), Aldo-keto reductase family 1 member C1 (*AKR1C1*), Thioredoxin reductase 1 (*TXNRD1*) and glyceraldehyde-3-phosphate dehydrogenase (*GAPDH*) genes was performed on a Viia 7 real-time PCR instrument (Applied Biosystems) using *Power* SYBR green PCR Master Mix (ThermoFisher). *GAPDH* was used as a normalization control. Primer sequences are detailed in Supplementary Table 1.

4.9. Reactive oxygen species (ROS) measurements

3D microtissue spheroids were incubated with varying concentrations of doxorubicin (Selleck Chemicals) for 48 h and ROS measured using the ROS-Glo H_2O_2 Assay (Promega) as described by the manufacturer's instructions. 100 μM Dexrazoxane was added 3 h and 100 nM CDDO-me or 10 μM sulforaphane, 24 h prior to doxorubicin incubation.

Author contribution statement

PS designed the study and LT, RB and PS wrote the manuscript text. ZQL carried out bioinformatics analysis and prepared Fig. 4. PS, HEC, CM, IC, MJC guided experiments. SDW carried out mathematical modelling and prepared Fig. 2. All authors reviewed and edited the manuscript.

Competing financial interests

The authors declare no competing financial interests.

Acknowledgments

We acknowledge the Liverpool Centre for Cell Imaging (CCI) for provision of imaging equipment and technical assistance. We would also like to thank Marco Marcello for help with technical assistance and image analysis support. The authors thank Alison Beckett and the electron microscope imaging facility at the University of Liverpool for providing expert technical support. We are grateful to Dr Deborah Simpson, from the Liverpool Centre for Proteome Research, for completing the proteomic analyses. This research was supported by institutional funding by the University of Liverpool. The proteomics analysis was supported in part by a grant from the Technology Directorate of the University of Liverpool. SDW acknowledges funding support from the Liverpool Centre for Mathematics in Healthcare (EPSRC grant: EP/N014499/1).

Appendix A. Supplementary data

Supplementary material related to this article can be found, in the online version, at doi:https://doi.org/10.1016/j.biopha.2019.108637.

References

[1] P.W. Burridge, et al., Human induced pluripotent stem cell-derived cardiomyocytes recapitulate the predilection of breast cancer patients to doxorubicin-induced cardiotoxicity, Nat. Med. 22 (5) (2016) 547–556.
[2] S.M. Swain, F.S. Whaley, M.S. Ewer, Congestive heart failure in patients treated with doxorubicin, Cancer 97 (11) (2003) 2869–2879.
[3] S.E. Lipshultz, et al., Cardiovascular disease in adult survivors of childhood Cancer, Annu. Rev. Med. 66 (2015) 161–176.
[4] J. Akam-Venkata, V.I. Franco, S.E. Lipshultz, Late cardiotoxicity: issues for childhood Cancer survivors, Curr. Treat. Options Cardiovasc. Med. 18 (7) (2016) 47.
[5] J.W. Yester, B. Kühn, Mechanisms of cardiomyocyte proliferation and differentiation in development and regeneration, Curr. Cardiol. Rep. 19 (2) (2017) 13.
[6] L. Zhao, B. Zhang, Doxorubicin induces cardiotoxicity through upregulation of death receptors mediated apoptosis in cardiomyocytes, Sci. Rep. 7 (2017) 44735.
[7] A.D. Hanna, et al., Adverse effects of doxorubicin and its metabolic product on cardiac RyR2 and SERCA2A, Mol. Pharmacol. 86 (4) (2014) 438–449.
[8] T. Eschenhagen, et al., Cardiovascular side effects of cancer therapies: a position statement from the Heart Failure Association of the European Society of Cardiology, Eur. J. Heart Fail. 13 (1) (2011) 1–10.
[9] T. Nousiainen, et al., Early decline in left ventricular ejection fraction predicts doxorubicin cardiotoxicity in lymphoma patients, Br. J. Cancer 86 (11) (2002) 1697–1700.
[10] D. Cardinale, et al., Early detection of anthracycline cardiotoxicity and improvement with heart failure therapy, Circulation 131 (22) (2015) 1981–1988.
[11] N. Milani-Nejad, P.M.L. Janssen, Small and large animal models in cardiac contraction research: advantages and disadvantages, Pharmacol. Ther. 141 (3) (2014) 235–249.
[12] E.L. Vegter, et al., Rodent heart failure models do not reflect the human circulating microRNA signature in heart failure, PLoS One 12 (5) (2017) p. e0177242.
[13] M. Bellin, C.L. Mummery, Stem cells: the cancer's gone, but did chemotherapy damage your heart? Nat. Rev. Cardiol. 13 (7) (2016) 383–384.
[14] Y. Octavia, et al., Doxorubicin-induced cardiomyopathy: from molecular mechanisms to therapeutic strategies, J. Mol. Cell. Cardiol. 52 (6) (2012) 1213–1225.
[15] S.K. Bjelogrlic, et al., Activity of d,l-α-Tocopherol (Vitamin e) against cardiotoxicity induced by doxorubicin and doxorubicin with cyclophosphamide in mice, Basic Clin. Pharmacol. Toxicol. 97 (5) (2005) 311–319.
[16] I.M. Copple, et al., NRF2 as an emerging therapeutic target, Oxid. Med. Cell. Longev. 2017 (2017) 2.
[17] Q. Ma, Role of Nrf2 in oxidative stress and toxicity, Annu. Rev. Pharmacol. Toxicol. 53 (2013) 401–426.
[18] L.M. Shelton, et al., Integrated transcriptomic and proteomic analyses uncover regulatory roles of Nrf2 in the kidney, Kidney Int. 88 (6) (2015) 1261–1273.
[19] N.R. Kitteringham, et al., Proteomic analysis of Nrf2 deficient transgenic mice reveals cellular defence and lipid metabolism as primary Nrf2-dependent pathways in the liver, J. Proteomics 73 (8) (2010) 1612–1631.
[20] T.E. Sussan, et al., Targeting Nrf2 with the triterpenoid CDDO- imidazolide attenuates cigarette smoke-induced emphysema and cardiac dysfunction in mice, Proc. Natl. Acad. Sci. 106 (1) (2009) 250–255.
[21] Y.-Y. Wang, et al., Bardoxolone methyl (CDDO-Me) as a therapeutic agent: an update on its pharmacokinetic and pharmacodynamic properties, Drug Des. Devel. Ther. 8 (2014) 2075–2088.
[22] H. Shah, et al., Protection of HepG2 cells against acrolein toxicity by 2-cyano-3,12-dioxooleana-1,9-dien-28-imidazolide via glutathione-mediated mechanism, Exp. Biol. Med. 240 (10) (2015) 1340–1351.
[23] Z. Xu, et al., Broccoli sprout extract prevents diabetic cardiomyopathy via Nrf2 activation in db/db T2DM mice, Sci. Rep. 6 (2016) 30252.
[24] M. Valentini, G. Parati, Variables influencing heart rate, Prog. Cardiovasc. Dis. 52 (1) (2009) 11–19.
[25] E. Laskowski, What's a normal resting heart rate? (Expert opinion), Mayo Clinic, Rochester, Minn, (2015) Available from: http://www.mayoclinic.org/healthy-lifestyle/fitness/expert-answers/heart-rate/faq-20057979.
[26] M. Tiburcy, et al., Terminal differentiation, advanced organotypic maturation, and modeling of hypertrophic growth in engineered heart tissue, Circ. Res. 109 (10) (2011) 1105–1114.
[27] J. England, S. Loughna, Heavy and light roles: myosin in the morphogenesis of the heart, Cell. Mol. Life Sci. 70 (7) (2013) 1221–1239.
[28] D. Hailstones, et al., Differential regulation of the atrial isoforms of the myosin light chains during striated muscle development, J. Biol. Chem. 267 (32) (1992) 23295–23300.
[29] P. Sharma, et al., Evolutionarily conserved intercalated disc protein Tmem65 regulates cardiac conduction and connexin 43 function, Nat. Commun. 6 (2015) 8391.
[30] D.A. Arvanitis, et al., Histidine-rich Ca-binding protein interacts with sarcoplasmic reticulum Ca-ATPase, Am. J. Physiol. - Heart Circ. Physiol. 293 (3) (2007) H1581–H1589.
[31] D.A. Arvanitis, et al., Histidine-rich calcium binding protein: the new regulator of sarcoplasmic reticulum calcium cycling, J. Mol. Cell. Cardiol. 50 (1) (2011) 43–49.
[32] M.J. Birket, et al., Expansion and patterning of cardiovascular progenitors derived from human pluripotent stem cells, Nat. Biotechnol. 33 (9) (2015) 970–979.
[33] A.I. Su, et al., A gene atlas of the mouse and human protein-encoding transcriptomes, Proc. Natl. Acad. Sci. U. S. A. 101 (16) (2004) 6062–6067.
[34] Z.Q. Lu, et al., Proteomic analysis of human fetal Atria and ventricle, J. Proteome Res. 13 (12) (2014) 5869–5878.
[35] A. Singh, et al., Small molecule inhibitor of NRF2 selectively intervenes therapeutic resistance in KEAP1-deficient NSCLC tumors, ACS Chem. Biol. 11 (11) (2016) 3214–3225.
[36] D. Jain, et al., Cardiac complications of Cancer therapy: pathophysiology, identification, prevention, treatment, and future directions, Curr. Cardiol. Rep. 19 (5) (2017) 36.
[37] D. Zujur, et al., Three-dimensional system enabling the maintenance and directed differentiation of pluripotent stem cells under defined conditions, Sci. Adv. 3 (5) (2017).
[38] H. Gaskell, et al., Characterization of a functional C3A liver spheroid model, Toxicol. Res. 5 (4) (2016) 1053–1065.
[39] K. Duval, et al., Modeling Physiological Events in 2D vs. 3D Cell Culture, Physiology 32 (4) (2017) 266–277.
[40] J.A. Kyffin, et al., Impact of cell types and culture methods on the functionality of in vitro liver systems – a review of cell systems for hepatotoxicity assessment, Toxicol. In Vitro 48 (2018) 262–275.
[41] H.K. Bryan, et al., The Nrf2 cell defence pathway: Keap1-dependent and -independent mechanisms of regulation, Biochem. Pharmacol. 85 (6) (2013) 705–717.
[42] W.A. LaFramboise, et al., Cardiac fibroblasts influence cardiomyocyte phenotype in vitro, Am. J. Physiol. - Cell Physiol. 292 (5) (2007) C1799–C1808.
[43] X. Yang, L. Pabon, C.E. Murry, Engineering adolescence: maturation of human

pluripotent stem cell–derived cardiomyocytes, Circ. Res. 114 (3) (2014) 511–523.
[44] C. Denning, et al., Cardiomyocytes from human pluripotent stem cells: From laboratory curiosity to industrial biomedical platform, Biochim. Biophys. Acta (BBA) – Mol. Cell Res. 1863 (7, Part B) (2016) 1728–1748.
[45] S.S. Nunes, et al., Biowire: a platform for maturation of human pluripotent stem cell-derived cardiomyocytes, Nat. Meth. 10 (8) (2013) 781–787.
[46] S.M. Swain, et al., Cardioprotection with dexrazoxane for doxorubicin-containing therapy in advanced breast cancer, J. Clin. Oncol. 15 (4) (1997) 1318–1332.
[47] S.E. Lipshultz, et al., The effect of dexrazoxane on myocardial injury in Doxorubicin-Treated Children with acute lymphoblastic leukemia, N. Engl. J. Med. 351 (2) (2004) 145–153.
[48] S.E. Lipshultz, et al., Treatment-related cardiotoxicity in survivors of childhood cancer, Nat. Rev. Clin. Oncol. 10 (12) (2013) 697–710.
[49] K.K. Hutchins, et al., Prevention of cardiotoxicity among survivors of childhood cancer, Br. J. Clin. Pharmacol. 83 (3) (2017) 455–465.
[50] P. Reichardt, et al., Risk-benefit of dexrazoxane for preventing anthracycline-related cardiotoxicity: re-evaluating the European labeling, Future Oncol. 14 (25) (2018) 2663–2676.
[51] K. Leger, et al., Subclinical cardiotoxicity in childhood cancer survivors exposed to very low dose anthracycline therapy, Pediatr. Blood Cancer 62 (1) (2015) 123–127.
[52] M. Volkova, R. Russell, Anthracycline cardiotoxicity: prevalence, pathogenesis and treatment, Curr. Cardiol. Rev. 7 (4) (2011) 214–220.
[53] P. Vachhani, et al., Dexrazoxane for cardioprotection in older adults with acute myeloid leukemia, Leuk. Res. Rep. 7 (2017) 36–39.
[54] K.T. Liby, M.M. Yore, M.B. Sporn, Triterpenoids and rexinoids as multifunctional agents for the prevention and treatment of cancer, Nat. Rev. Cancer 7 (5) (2007) 357–369.
[55] A. MacLeod, et al., Characterization of the cancer chemopreventive NRF2-dependent gene battery in human keratinocytes: demonstration that the KEAP1–NRF2 pathway, and not the BACH1–NRF2 pathway, controls cytoprotection against electrophiles as well as redox-cycling compounds, Carcinogenesis 30 (9) (2009) 1571–1580.
[56] D. Ross, D. Siegel, Functions of NQO1 in cellular protection and CoQ(10) metabolism and its potential role as a redox sensitive molecular switch, Front. Physiol. 8 (2017) 595.
[57] S. Nishimoto, et al., Activation of Nrf2 attenuates carbonyl stress induced by methylglyoxal in human neuroblastoma cells: increase in GSH levels is a critical event for the detoxification mechanism, Biochem. Biophys. Res. Commun. 483 (2) (2017) 874–879.
[58] D. de Zeeuw, et al., Bardoxolone methyl in type 2 diabetes and stage 4 chronic kidney disease, N. Engl. J. Med. 369 (26) (2013) 2492–2503.
[59] M.P. Chin, et al., Risk factors for heart failure in patients with type 2 diabetes mellitus and stage 4 chronic kidney disease treated with bardoxolone methyl, J. Card. Fail. 20 (12) (2014) 953–958.
[60] C. Angeloni, et al., Modulation of phase II enzymes by sulforaphane: implications for its cardioprotective potential, J. Agric. Food Chem. 57 (12) (2009) 5615–5622.
[61] J.J. Alumkal, et al., A phase II study of sulforaphane-rich broccoli sprout extracts in men with recurrent prostate cancer, Invest. New Drugs 33 (2) (2015) 480–489.
[62] S.M. Ravenscroft, et al., Cardiac non-myocyte cells show enhanced pharmacological function suggestive of contractile maturity in stem cell derived cardiomyocyte microtissues, Toxicol. Sci. 152 (1) (2016) 99–112.
[63] K. Sekine, et al., Oxygen consumption of human heart cells in monolayer culture, Biochem. Biophys. Res. Commun. 452 (3) (2014) 834–839.
[64] R.J. Shipley, et al., A strategy to determine operating parameters in tissue engineering hollow fiber bioreactors, Biotechnol. Bioeng. 108 (6) (2011) 1450–1461.
[65] J. Leedale, et al., Modeling the dynamics of hypoxia inducible factor-1α (HIF-1α) within single cells and 3D cell culture systems, Math. Biosci. 258 (2014) 33–43.